Liquid Crystal Peptide/DNA Coacervates in the Context of Prebiotic Molecular Evolution

Tony Z. Jia [1,2,*,†] and **Tommaso P. Fraccia** [3,*,†]

1   Earth-Life Science Institute, Tokyo Institute of Technology, 2-12-1-IE-1 Ookayama, Meguro-ku, Tokyo 152-8550, Japan

2   Blue Marble Space Institute of Science, 1001 4th Ave., Suite 3201, Seattle, WA 98154, USA

3   Institut Pierre-Gilles de Gennes, CBI, ESPCI Paris, Université PSL, CNRS, 75005 Paris, France

*   Correspondence: tzjia@elsi.jp (T.Z.J.); tommaso.fraccia@espci.fr (T.P.F.)

†   These authors contributed equally.

Abstract: Liquid–liquid phase separation (LLPS) phenomena are ubiquitous in biological systems, as various cellular LLPS structures control important biological processes. Due to their ease of in vitro assembly into membraneless compartments and their presence within modern cells, LLPS systems have been postulated to be one potential form that the first cells on Earth took on. Recently, liquid crystal (LC)-coacervate droplets assembled from aqueous solutions of short double-stranded DNA (s-dsDNA) and poly-L-lysine (PLL) have been reported. Such LC-coacervates conjugate the advantages of an associative LLPS with the relevant long-range ordering and fluidity properties typical of LC, which reflect and propagate the physico-chemical properties of their molecular constituents. Here, we investigate the structure, assembly, and function of DNA LC-coacervates in the context of prebiotic molecular evolution and the emergence of functional protocells on early Earth. We observe through polarization microscopy that LC-coacervate systems can be dynamically assembled and disassembled based on prebiotically available environmental factors including temperature, salinity, and dehydration/rehydration cycles. Based on these observations, we discuss how LC-coacervates can in principle provide selective pressures effecting and sustaining chemical evolution within partially ordered compartments. Finally, we speculate about the potential for LC-coacervates to perform various biologically relevant properties, such as segregation and concentration of biomolecules, catalysis, and scaffolding, potentially providing additional structural complexity, such as linearization of nucleic acids and peptides within the LC ordered matrix, that could have promoted more efficient polymerization. While there are still a number of remaining open questions regarding coacervates, as protocell models, including how modern biologies acquired such membraneless organelles, further elucidation of the structure and function of different LLPS systems in the context of origins of life and prebiotic chemistry could provide new insights for understanding new pathways of molecular evolution possibly leading to the emergence of the first cells on Earth.

Keywords: liquid crystals; complex coacervation; phase separation; supramolecular assembly; membraneless organelles; origins of life; protocell; DNA self-assembly; prebiotic chemistry; molecular chemical evolution

1. Introduction

Modern cells are composed of a complex conglomerate of various small molecules, proteins, and phospholipids. How these cells initially emerged and assembled still remains a mystery. It has been proposed that primitive cells were liposomes composed of a simple fatty acid bilayer, possibly oleic acid, which enclosed genetic polymers and catalysts [1]. Such a compartmentalization strategy

may be necessary as it prevents the diffusion of genetic and catalytic materials out of the compartment, while also preventing replicating parasites from overtaking such a system [2] and still allowing the import and export of small nutrients and byproducts [3]. While such primitive bilayer systems clearly provide essential functions, fatty acid bilayer vesicles were likely not the only compartment system capable of assembly on early Earth [4,5].

While searching for non-vesicular compartments that could have existed on early Earth, researchers have taken inspiration from droplets and compartments assembled from liquid–liquid phase separation (LLPS) within modern cells, which perform various functions such as segregation of analytes, housing of important reactions, or regulation [6,7]. Although it is unclear whether such droplets were a recent evolutionary achievement or are conserved throughout history, the fact that many essential cellular functions are regulated by LLPS may suggest their importance to primitive biologies as well. Nevertheless, researchers have been able to produce such LLPS droplets in the laboratory from a variety of materials, both natural and synthetic [8–11]. In particular, complex coacervate droplets are one type of LLPS of interest for origins of life researchers due to the relative ease of the synthesis of their components (these can be assembled from simple monomers and polymers such as nucleotides (and nucleic acids), amino acids (and peptides), polyesters, and polyamines [12–16]). Although such coacervate droplets have not been shown to be direct ancestors of modern or primitive cells, this does not exclude their potential to have participated in primitive chemistries and biochemistries whether as protocells themselves, or simply as compartments which played orthogonal roles such as through lipid layer scaffolding or assembly [17], as primitive microreactors [14], or compartmentalization of catalytic and genetic molecules [18,19]. Complex coacervates are associative phase separated systems where electrostatic binding of multiple oppositely-charged polyions results in the formation of two co-existing liquid phases, one of which is a polymer-depleted dilute bulk phase and one of which is the condensed coacervate phase, enriched in both polymers, which still contains high water content [20]. Such phase separation is fundamentally different from precipitation as precipitates do not contain much water content. Coacervate assembly can also controlled by various environmental factors such as pH, ionic strength, temperature (T), and the concentration (and length) of the components [21,22]. Thus, if coacervates were present on early Earth and participated in primitive chemistries, environmental changes (T, pH, ionic strength, etc.) caused by diurnal, seasonal, or precipitation cycles [23] are proposed to have driven the assembly (and disassembly) of such droplets [24].

Of the various coacervate compositions, peptide-nucleic acid coacervates can be produced from biomolecules likely to have existed on early Earth, i.e., simple cationic peptides and nucleotides (or nucleic acids). Amino acids can be produced from primitive atmospheric discharge [25] or delivered to Earth from extraterrestrial meteorites [26], while peptides could have been polymerized on early Earth through various methods such as on mineral surfaces [27] or via a depsipeptide intermediate [28]. On the other hand, components of nucleotides such as ribose, the main sugar component of RNA, and nucleobases have been identified on meteorites [29], and laboratory simulations have shown a plausible way for each nucleotide to be synthesized prebiotically [30]. Nucleic acids can then in turn be polymerized through wet-dry cycling of nucleotides on mineral surfaces [31] or through non-enzymatic chemical oligomerization [32]. Assembled and polymerized nucleotides (i.e., RNA) in particular have been proposed to be the first primitive biopolymers, as part of the RNA World theory, due to their ability to carry and transmit genetic information and to function as catalysts through ribozymes [33]. Although replicating RNA systems utilizing non-enzymatic polymerization have been proposed and demonstrated in the laboratory [32], recent research has suggested that chimeric DNA/RNA systems may have been the preferred form of primitive replicating nucleic acid systems on early Earth [34]. This finding suggests that at some point in history, perhaps DNA and RNA co-existed on early Earth. Assuming such co-existence (also with cationic peptides), then it is plausible that both peptide-RNA and peptide-DNA coacervates could have existed on early Earth.

Primitive peptide-DNA coacervates are interesting to consider in particular due to the DNA's ability to assemble into very unique macromolecular structured phases such as DNA

origamis [35–37] or liquid crystals (LCs) [38–41]. Typical lyotropic LC phases can be produced in highly concentrated aqueous solutions of long DNA polymers [42], but also of short DNA and RNA oligomers (s-dsDNA/RNA) [38,39,43–46], depending on the sequence and the solution conditions, or monomers [40] and have been observed intracellularly [47]. In particular, LC ordering requires high polymer rigidity, as observed in long double-stranded DNA or RNA (dsDNA and dsRNA, respectively) [48], or generated by the formation of linear aggregates of end-to-end interacting s-dsDNA or single nucleotides, which in turn order into LC phases following a chromonic type behavior [46]. These LCs, by definition, provide a partially ordered phase, but maintain the fluidity that is typical of an unstructured liquid phase. Such a partially ordered LC phase has been shown to be applied towards scaffolding of chemical [49] or biological [50] structures, selective reaction control [51], modulating the chemical and physical properties of an existing surface or object [52], and inducing emergent viscoelastic properties in biomolecular materials [53–55]. Moreover, s-dsDNA/RNA LC phases have been proven to provide a templating matrix capable of enhancing non-enzymatic chemical reactions, such as ligation, involving their constituting building blocks: the LC order acts as the ligase enzyme by allowing close contact of the 3′- and 5′- termini of the nucleic acid fragments to be ligated [56–58]. Indeed, in the LC phase, oligomeric DNA or RNA fragments can be elongated more than 10 times their initial length (e.g., from 12 bases to more than 120) more efficiently as compared to normal liquid phases.

These demonstrations suggest that imparting LC ordering could be one way to efficiently generate enough long nucleic acid polymers to possibly display enzymatic activity (ribozymes), essential for a proposed RNA World to be initiated [33], or result in increased chemical or physical complexity of a primitive coacervate system, imparting selection or scaffolding of more functional components or structures. For example, assembly of a multiphase coacervate system has been shown through simple systematic mixing of complex polycation (polypeptide and polyamine) mixtures [59,60] or partially complementary DNA sequences [61], while DNA LC-containing coacervates have been studied theoretically [62] and experimentally [63,64]. Here, we discuss the relevance of DNA LC-coacervates in the context of prebiotic molecular evolution. The ability for LC-coacervates to significantly increase the concentration of the internal components, and also their stability through temperature and wet-dry cycles which simulate primitive Earth environmental processes were studied. These assays give insights into the ability of LC-coacervates to cyclically assemble, while also highlighting their structural and heat-stability, important considerations affecting their ability to undergo selective evolution. The structural complexity of dsDNA LC-coacervates may also provide a glimpse into how primitive genetic systems transitioned from single stranded to duplexed nucleic acid systems during the course of chemical evolution.

2. LC-Coacervate Structure and Local Nucleic Acid Concentration Increases

We investigated mixtures of cationic peptides (poly-L-lysine (PLL), MW 30–70 kDa, i.e., 240 residues), and a self-complementary oligomeric s-dsDNA 12-mer, 5′-GCGCTTAAGCGC-3′ (reverse Dickerson dodecamer, rDD), under charge-balanced conditions (i.e., the total concentration of positive charges from PLL amino groups (N) were equivalent to the total concentration of negative charges from rDD phosphate groups (P); N = P = 10 mM), for simultaneous coacervation and LC ordering ability [63]. LC-coacervates could be assembled upon mixing of the s-dsDNA, which forms stiff linear aggregates upon end-to-end stacking of duplexes, and PLL in the presence of monovalent salt, in this case, sodium chloride (NaCl) (Figure 1A). We observed that varying concentrations of NaCl affected both coacervation and LC formation, likely due to affecting the strength of the electrostatic-driven complexation between the peptide and DNA [65]. In particular, coacervates showing all known DNA LC mesophases were observed through brightfield (BFTOM) and polarized (PTOM) transmission optical microscopy at various NaCl concentrations (Figure 1B): isotropic (ISO) coacervates at 900 mM NaCl resulting mainly from electrostatic complexation between short aggregates of s-dsDNA and PLL (Figure 1C), cholesteric (N*) LC-coacervates at 800 mM NaCl resulting from electrostatic binding

and assembly of long aggregates of end-to-end stacked rDD which order in twisted nematic planes (Figure 1D), uniaxial columnar (C_U) LC-coacervates at 700 mM NaCl resulting from hexagonal packing of the long end-to-end stacked rDD-PLL assemblies which still maintain the capability to bend (Figure 1E), and higher-order columnar (C_2) LC-coacervates at 600 mM NaCl resulting from tight hexagonal packing of the long end-to-end stacked rDD-PLL assemblies where bending is suppressed (Figure 1F). LC phases were identified through texture recognition of PTOM images, as has been established previously in both LC-coacervates [63] and bulk s-dsDNA [43]. Salt concentrations above 900 mM resulted in the permanence of the system in a uniform phase [63], meaning that the critical salt concentration for coacervation, [NaCl]*, was overcome.

During the last decade, s-dsDNA/RNA LC have been proposed as an intriguing pathway, based on self-assembly, for the formation of polymeric nucleic acids from oligomers or monomers [56–58]. The unsolved problem with this hypothesis is the fact that prebiotic environments usually result in fairly low concentrations (µM or low mM range) of nucleic acid fragments, conceivably mostly single nucleotides [66], while LC can arise only at far higher DNA/RNA concentrations between 300 mg/mL (for 12 bp DNA oligomers, i.e., ~80 mM) [67] and 800 mg/mL (for mixtures of deoxyadenosine triphosphate (dATP) and deoxythymidine triphosphate (dTTP), i.e., ~1.5 M) [40]. Even if such concentrations cannot likely be found on prebiotic Earth, these values are in the range of the DNA concentration of chromatin in modern cell nuclei [68]. Moreover, much higher concentrations than prebiotic ones are often required for biological or life-like functions, such as polymerization or catalysis. Thus, efficient mechanisms to increase molecular concentration have been always sought by origins of life investigators, as a means to overcome reactant and catalyst concentration limitations in primitive systems.

In this frame, given the nature of associative phase separation, coacervation has the ability to locally concentrate nucleic acid and peptide polymers in the dense coacervate phase, starting even from a solution prepared at much lower global concentration [16]. For example, the reported LC-coacervates were obtained in solutions prepared at an initial DNA concentration of just 3.3 mg/mL, which corresponds to 0.91 mM, i.e., 10 mM total negative charges divided by 11 charges for each 12-mer strand (grey dashed line in Figure 1B). We next measured the DNA concentration within the dense coacervate droplets as well as in the diluted continuous phase (*Methods*) in order to identify the biphasic region and the binodal line (light purple shading and solid purple line in Figure 1B). As normally observed for coacervation, the binodal line was found to be asymmetric with a very sharp decay of the left arm, corresponding to the border of diluted phase (open symbols), and a very broad decay of the right arm, corresponding to the concentration of the dense phase (filled symbols). This implies that lowering [NaCl], which corresponds to higher DNA-PLL complexation due to decreased electrostatic interaction screening, induces greater DNA enrichment within the coacervate droplets, the latter explaining the transitions between the different LC mesophases as normally observed in bulk DNA systems, where the crucial parameter is DNA concentration. Such behavior is easily understood by considering the increasing degree of order between the different mesophases, going from ISO to N* to C_U to C_2, as a response to the increasing volume fraction of the DNA-PLL bundles in the dense coacervate phase.

In general, when compared to the initial DNA concentration, all coacervate phases were able to enrich DNA by around two/three orders-of-magnitude (i.e., ~100/1000-fold) into the dense droplet phase (Figure 1B). Similar to what has been shown in other primitive coacervate systems [16], this demonstration suggests that LC-coacervates are one possible mechanism by which primitive nucleic acid concentration could be significantly enriched on prebiotic Earth, increasing in concentration from an inactive, but prebiotically plausible regime (less than millimolar), to a higher concentration regime where nucleic acids could more readily perform life-like functions (hundreds of millimolar).
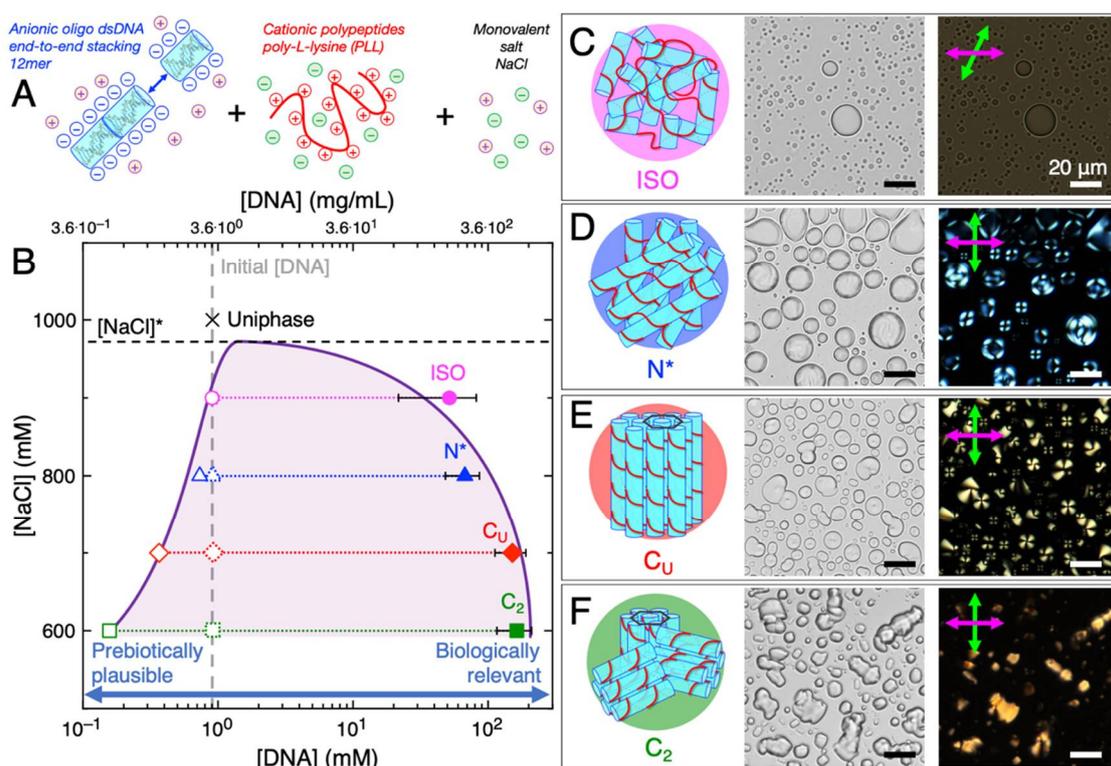
Figure 1. Liquid crystal (LC)-coacervate phase diagram and structure as function of [NaCl]. (**A**) Mixing of an anionic s-dsDNA 12-mer (reverse Dickerson dodecamer (rDD), 5'-GCGCTTAAGCGC-3') capable of end-to-end stacking with a 240-residue cationic peptide (poly-L-lysine, PLL) in the presence of a monovalent salt (sodium chloride, NaCl) resulted in assembly of LC-coacervates. (**B**) Phase diagram of mixtures of rDD and PLL (N = P = 10 mM) as a function of [DNA] and [NaCl]. The initial preparation (DNA = 0.91 mM ~ 3.3 mg/mL) is identified by the vertical grey dashed line and dashed open symbols. Below a critical salt concentration, [NaCl]* (horizontal black dashed line), the system de-mixes in a dense coacervate phase (filled symbols) coexisting with a diluted liquid phase (open symbols). The dense inner coacervate phase shows different degrees of order as function of [NaCl]: isotropic (ISO) at 900 mM NaCl (magenta circle), cholesteric (N*) at 800 mM NaCl (blue triangle), uniaxial columnar (C_U) at 700 mM NaCl (red diamond), and higher-order columnar (C_2) at 600 mM NaCl (green square). At 1 M NaCl, the system existed as a uniform phase (black cross). The measured DNA concentration (*Methods*) testifies a ~100/1000-fold DNA enrichment in the dense coacervate phase. Error bars indicate standard mean error. A qualitative binodal line (solid purple line), dividing the diagram in a two-phase-region (purple shading) and a uniphase region (white), was drawn by interpolating the datapoints with a spline. Hypothetical tie lines (horizontal dotted lines) have also been reported. Coacervation is shown to enrich [DNA] from prebiotically plausible regimes to LC enabling and biologically relevant regimes. (**C**–**F**) Sketches of the inner structure and optical microscopy images of the observed coacervates phases: ISO characterized by optically inactive droplets of disordered liquid DNA-PLL complexes (**C**), N* characterized by typical fingerprint textures formed by twisted nematic planes of DNA-PLL complexes (**D**), C_U characterized by focal conic structures formed by bending-prone two-dimensional hexagonally ordered DNA-PLL complexes (**E**), and C_2 characterized by more uniform and sharp-edged birefringent domains given by tight hexagonal order of DNA-PLL complexes where bending is suppressed (**F**). Middle: brightfield transmission optical microscope (BFTOM) image. Right: polarized transmission optical microscopy (PTOM) image. Scale bars are 20 μm.

3. Comparison of ISO and LC-Coacervate Stability versus Temperature

One major physical variable aside from salinity that affects the structure of an LC-coacervate is temperature. Previously, it was observed that higher temperatures dissociate the LC-coacervate, while

cooling reconstitutes the original LC structure or causes the replacement of precipitates with C_U and C_2 phases) depending on the NaCl concentration [63]. Given that heat cycles are crucial environmental processes that drove prebiotic chemistries, we were interested in further probing the effect of such heat cycles on the DNA LC-coacervate [69].

We first allowed rDD/PLL coacervate droplets to form at room temperature (N = P = 10 mM) under two conditions, one which exhibited N* coacervates (800 mM NaCl) and one which did not exhibit LC assembly and formed only ISO droplets (900 mM NaCl). We then slowly increased the temperature of these samples up to 50 °C and observed their thermal stability through fluorescence and polarization microscopy (Figure 2). For the LC-coacervate droplets (Figure 2A), we observed through polarization microscope images that the LC phase began to disassemble upon mild heating to 30 °C, eventually completely disappearing at 35 °C. However, the coacervate droplets themselves remained stable up to higher temperatures, and between 40 °C and 50 °C the coacervate droplets began to disassemble, as evidenced by their slight decrease in size and abundance. In contrast, ISO coacervate droplets (Figure 2B) were stable only up to 30 °C; from 40 °C, the droplets disassembled rapidly, as evidenced by their significance decrease in size and the disappearance of most droplets. It is likely that the additional NaCl resulted in greater destabilization of the rDD-PLL interaction, resulting in a lower temperature of rDD-PLL dissociation; a similar effect was observed in a previous study, where higher NaCl concentrations resulted in lower temperatures of coacervate dissociation [63].

After both samples were heated to 50 °C, they were cooled back to 25 °C. LC phase-containing droplets retained their original size and number (Figure 2C), while the ISO droplets did not appear to recover their size to an appreciable degree (Figure 2D). A direct comparison of average droplet size and the ratio of area covered by the droplets (within the viewing frame) of both samples after heating to different temperatures is plotted in Figure 2E,F, respectively, while the crosses note the relevant values of each sample after cooling back down to 25 °C after heating to 50 °C. The fact that the LC-containing droplets did not completely disassemble upon heating to 50 °C (Figure 2A), rather simply slightly decreasing in size and number, may have allowed the remaining smaller droplets to act as nucleation seeds for free peptides and DNA to "re-coacervate".

ISO droplets did not appear to recover their initial size potentially due to the fact that the reassembly of the coacervate phase can be affected if NaCl concentration increased slightly during the thermal treatment due to slight water evaporation, even if samples were sealed with mineral oil or plastic coverings to reduce evaporation (Methods). This effect is more evident for the ISO coacervates since their initial NaCl concentration is closer to the $[NaCl]^*$.

Even if re-nucleation of the coacervates droplets can highly depend on thermal history and temperature variation rates, these observations suggest that, in the investigated conditions, the LC-coacervates are more heat-stable than ISO coacervates due to an additional contribution to structural stability by an ordered LC phase; the exact mechanism is beyond the scope of this study. Greater heat-stability and ability to reassemble after total or partial disassembly would be a selective advantage for LC-coacervates, potentially resulting in their greater chance of survival and persistence (and subsequent potential for evolution) in a primitive environment with mild temperature fluctuations compared to their non-LC-forming counterparts.

An expanded study on LC-coacervate phase dependence on temperature was performed, showing the ability for a LC-coacervate system to transition through various phases (precipitation, to LC-coacervate droplet, to isotropic coacervate droplet, to a uniform phase) continuously upon increases in temperature at various salinities (Figure 3A), with increased temperatures first resulting in disassembly of the LC mesophase (caused by end-to-end s-dsDNA duplex stacking) followed by disassembly of the coacervate droplet itself (caused by electrostatic binding between the peptide and DNA).
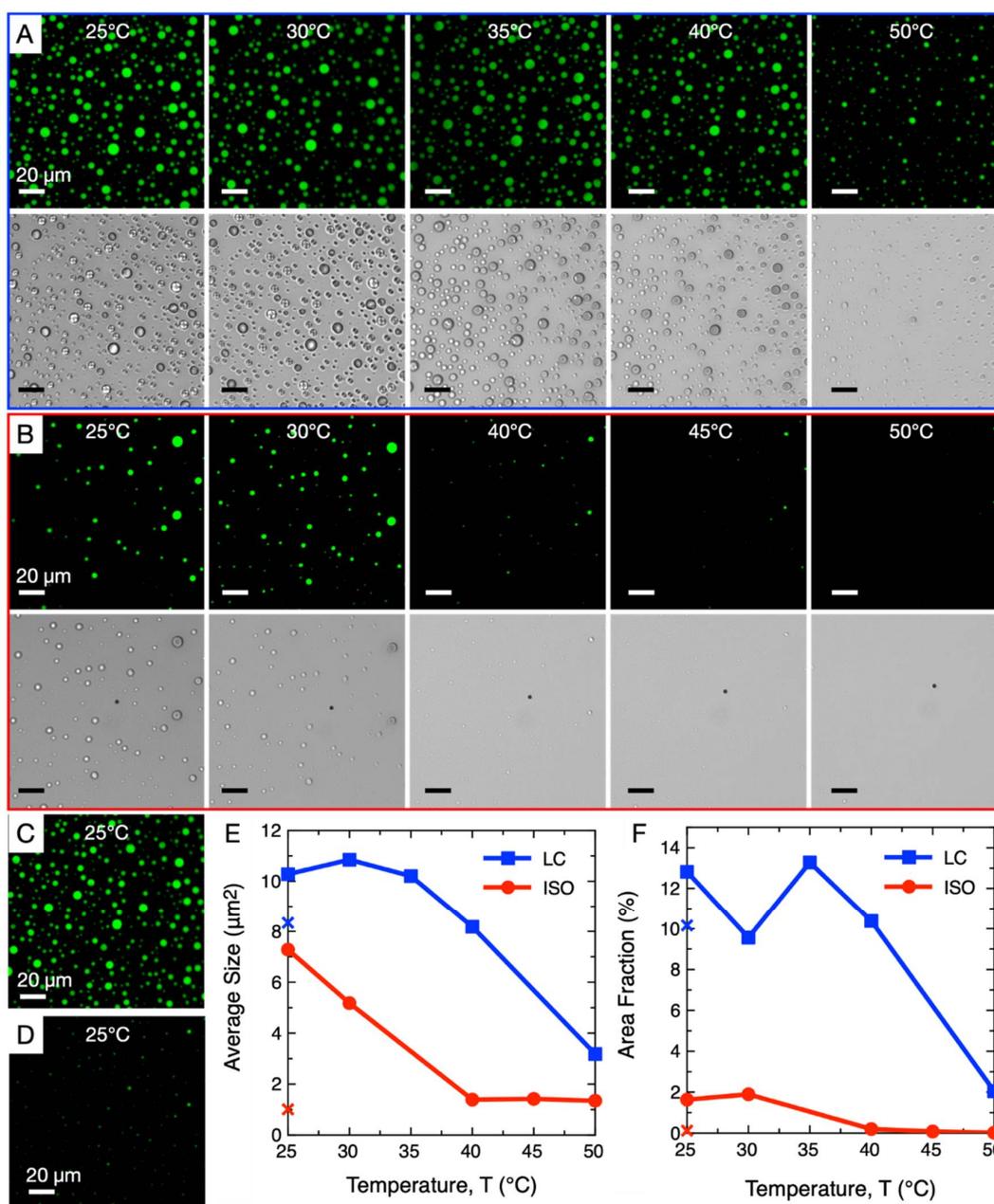
Figure 2. Thermal stability of LC-coacervates and LC phase-lacking isotropic coacervates. (**A**) Fluorescence (top, SYBR Gold) and polarization (bottom) microscopy images of PLL (N = 10 mM) and rDD (P = 10 mM) coacervate droplets at 800 mM NaCl exhibiting LC phase assembly undergoing heating up to 50 °C. (**B**) Fluorescence (top, SYBR Gold) and polarization (bottom) microscopy images of PLL (N = 10 mM) and rDD (P = 10 mM) coacervate droplets at 900 mM NaCl, exhibiting no LC phase assembly (isotropic), undergoing heating up to 50 °C. (**C**) A LC-coacervate sample from (**A**), after heating to 50 °C (slight disassembly), was returned to 25 °C and imaged. The sample re-assembled into coacervate droplets roughly similar in size to their original size before heating. (**D**) An ISO coacervate sample from (**B**), after heating to 50 °C (slight disassembly), was returned to 25 °C and imaged. The sample did not appear to reassemble into coacervate droplets. (**E**,**F**) Average size (**E**) and total droplet area within the viewing frame (**F**) vs. T of both samples, LC phase-containing (blue squares) and ISO droplets (red dots). The crosses represent the average size and total droplet area (within the viewing frame), respectively, of both samples (LC in red, ISO in blue) after reducing the temperature from 50 °C to 25 °C. Scale bars are 20 µm.

Generally, cooling allows the coacervate droplets to reassemble, if all of the other conditions (DNA, PLL, and NaCl concentration) are kept constant. At lower NaCl content, 600–700 mM, the columnar LC phases appeared from an initial birefringent precipitate state only after heating and cooling (i.e., temperature annealing) and suggests that annealing of a LC-coacervate system can result in accession of novel structures previously inaccessible without temperature cycling [63]. This suggests that geochemically driven temperature cycling on early Earth, possibly through thermophoretic gradients in oceanic rock pores [70] or transition into/out of hydrothermal vent systems in the deep ocean [71], could have also allowed primitive LC-coacervate systems to access novel structures, allowing for structural diversity/complexity and potentially novel function. NaCl concentrations below 600 mM were not investigated in this study, although it has been shown that in the absence of temperature annealing, precipitate structures dominate at room temperature below 600 mM NaCl; however, at 0 mM NaCl, even upon temperature annealing, the structure remains in the precipitate form [63].

4. Thermal Stability of LC-Coacervates

Both the LC phase and the entire coacervate droplet in a DNA/cationic peptide form from non-covalent interactions between the various polymers. LC phases require DNA hybridization followed by end-to-end stacking driven linear aggregation of short DNA duplexes [56], while coacervation requires electrostatic or hydrogen bonding interactions between the DNA and the peptide to effect entropy-driven phase separation [11,72] (Figure 3B). Each of these polymer-polymer interactions can be inhibited with temperature, depending on their free energy, ΔG. Even if precise free energy values are often difficult to evaluate both experimentally and theoretically, in particular when the different interactions can affect each other as in this case, we can consider some values reported in literature. Between them the lowest is surely the stacking interaction, with free energy ΔG_{stack} ~ −2 kcal/mol [67,73] (all ΔG values are evaluated at 37 °C). The thermodynamics of DNA hybridization has been widely investigated and robust models based on nearest neighbor parameters (NN models) [74] allow the prediction of the hybridization free energy ΔG_{hybr}, which for the case of 12 bp rDD is ~ −28 kcal/mol. Lastly, estimation of PLL/DNA binding has been obtained by molecular dynamics simulations, ΔG_{bind} ~ −7 kcal/mol for each lysine residue [75], even if such a quantitative result is affected considerably by model assumptions.

We experimentally observed that, upon heating of a DNA/PLL LC-coacervate system, the disassembly of LC ordering (LC T_M) is the first effect of increasing temperature (disappearance of birefringent textures in PTOM images in Figure 3B), this being in complete accordance with the estimations of DNA duplex end-to-end stacking interaction. A further temperature increase causes the disassembly of the whole coacervate droplet (coacervate T_M), which is observed around 50 °C in the reported example (Figure 3B) and is principally due to suppression of the DNA/PLL interactions, since coacervation would be maintained even in the presence of ssDNA [76]. Nevertheless, from simple bright field micrographs alone, it is not trivial to understand if DNA/PLL unbinding occurs or not upon melting of DNA duplexes, since ISO coacervates made of dsDNA or ssDNA are indistinguishable (BFTOM in Figure 3B).

However, theoretical predictions through NN models [74] place the DNA duplex melting temperature at [NaCl] = 800 mM and [rDD] = 0.91 mM to be around 75–80 °C, although contributions from PLL binding to DNA were not accounted for. Previous studies have observed slight DNA melting temperature increases upon peptide binding [77,78] and that basic amino acids contribute to greater duplex stability [79]. This suggests that ISO coacervates are principally composed by still-duplexed DNA, in this case capable of weak linear aggregation due to a suppressed end-to-end interaction, and that DNA de-hybridization takes place at higher temperature when the system is in the uniform phase. Since the coacervate T_M increases with decreasing [NaCl] (e.g., coacervate T_M > 90 ° C at [NaCl] = 600 mM), we cannot exclude that, at low [NaCl], DNA duplex melting could already be occurring in the ISO coacervate phase or even preceding coacervate disassembly.

5. Relevance of LC-Coacervates in Wet–Dry Cycles

It has been shown that LC-coacervate droplets disassemble (or transition to a different mesophase) when the salt concentration of the environment changes. One prebiotically plausible mechanism that could result in control of salt concentration is the dehydration rehydration cycle, also known as the wet-dry cycle [24]. Wet-dry cycles can occur geochemically through precipitation/evaporation events (caused by seasonal or diurnal cycles) [80] or through deliquescence [81]. The dehydration step drives the conjugation of primitive polymers through dehydration synthesis [15,30,81–83]. While the rehydration step allows synthesized polymers to undergo the reverse hydrolysis step to regenerate monomers and shorter oligomers. The repeated cyclical combination of dehydration (synthesis) followed by rehydration (hydrolysis) results in accumulation of only those polymers that are most stable to hydrolysis and can survive such a destructive environmental cycle [28]. Thus, it is believed that cyclical wet-dry cycles were crucial on early Earth to allow for polymeric chemical evolution [84,85].

Additionally, as wet-dry cycles are able to modulate analyte concentrations and salinities, they have been shown to potentially have played a role in the cyclical assembly and/or disassembly of primitive compartments, such as coacervates [24]. Upon subjecting a PLL/rDD mixed system, initially in a non-functional precipitate state, to dehydration, it was observed that eventual stepwise transitions into (potentially functional) LC-coacervate droplets, (potentially semi-functional) ISO droplets, and then to a non-functional uniform phase occurred (black arrows in Figure 3C). This was likely due to the fact that, although removal of water increased rDD and PLL concentrations, it also increased [NaCl], which resulted in the system being able to explore different regions of the phase diagram, eventually achieving conditions that allow the assembly of each of these mesophases. In fact, conceptually, one would initially think that further dehydration of a precipitate would not result in its dissociation, rather increasing its insolubility. However, it is possible that upon increasing rDD, PLL, and NaCl concentrations into a regime that allows formation of LC-coacervate droplets, the rDD and PLL molecules are more likely to rearrange out of a precipitate state and into the more stable LC-coacervate state. There may also be a "salting in" component, where the increased ionic strength from increase of [NaCl] results in a sufficient increase in solubility (due to decrease in rDD-PLL binding strength) at lower [NaCl] for the precipitate to dissociate. The entire drying/disassembly process can also occur in the reverse process through environmental wetting such as through precipitation, resulting in the system transitioning through all of the intermediate states in reverse order (green arrows in Figure 3C).

This environmental control, and especially the cyclical nature of salinity changes perhaps resulting in wet-dry cycles in coastal conditions (potentially coupled with temperature fluctuations mentioned previously), could allow the continued assembly and disassembly of LC-coacervates. Even if the [NaCl] fluctuations did not result in full disassembly of the system into a uniform phase, such a process could still allow an LC-coacervate system to access a larger space of possible phases at some point in time, potentially increasing its structural complexity and diversity, which could in turn increase functional complexity and diversity. Access to additional structures and functions through environmental cycling may apply even to systems which appear to start from or temporarily reconfigure to "non-functional" states such as a precipitate or a salt crystal. Assuming that LC-coacervate droplets could perform some essential primitive function such as biomolecule compartmentalization, geological cycling could provide the system the ability to "turn-on" or "turn-off" its function depending on the environmental conditions; this would be, in effect, a primitive functional switch (Figure 3C).
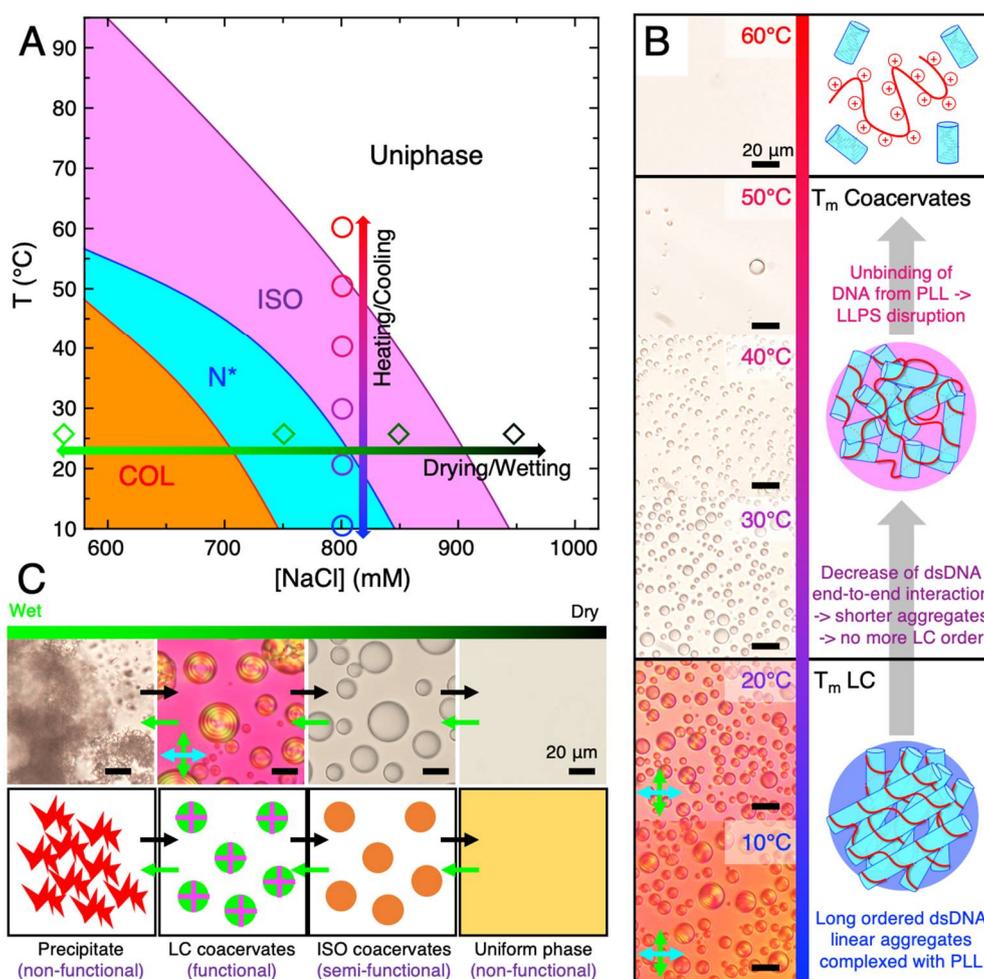
Figure 3. Stability of LC-coacervate phases in temperature and hydration cycles. (**A**) Phase diagram of the LC-coacervate system at different T and [NaCl]. Increasing temperature transitions the system between various mesophases such as from the columnar phases (COL), to N*, to ISO, and finally to a uniform phase. Modulation of the [NaCl] of a system, potentially through drying and wetting, also results in transition between the same phases. (**B**) PTOM and BFTOM images of the LC-coacervate system at various temperatures (corresponding to the color-coded empty circles in A), showing the transition between the mesophases upon heating. At low temperatures, the LC-coacervate phase exists due to the presence of enough long linear aggregates of s-dsDNA complexed with PLL (blue shaded sketch), while heating causes transition from LC to ISO coacervates as a consequence of the weakening of the s-dsDNA end-to-end interactions, resulting in less ordered and shorter s-dsDNA aggregates still complexed with PLL (magenta shaded sketch). Further heating results then in dissociation of the coacervate droplets and formation of the uniform phase, due to the unbinding of the DNA from the peptide. (**C**) PTOM and BFTOM images of dehydration of an rDD-PLL system at room temperature (corresponding to the color-coded empty diamonds in A). A continuous transition from precipitate, to LC-coacervate droplets, to ISO coacervate droplets, to a uniform phase occurred over the drying process, mainly due to the effect of the increasing [NaCl]. In this way, environmental dehydration and rehydration could result in continuous transitions between functional LC-coacervate or semi-functional isotropic coacervate states and non-functional precipitate or uniform phase states (sketches). Scale bars 20 μm.

6. Relevance of LC-Coacervates to Prebiotic Oceans

There have been a wide variety of suggestions as to where primitive life originated, including both oceanic environments as well as freshwater environments. However, if LC-coacervates were

to have participated in primitive biochemistries on early Earth, they likely would have necessarily resided in oceanic environments due to the requirement of high salinities relative to freshwater environments and physiological conditions for assembly. The salinity of the modern ocean is roughly 35 g/L, which corresponds to ~600 mM NaCl (this assumes that most of the salt is NaCl, although there are a number of other species present at lower concentrations) [86], and appears to suggest that some LC-coacervate phases are compatible with an ocean environment in the absence of temperature modulations (Figure 1) [63]. However, upon modulation of temperature, plausibly caused by seasonal or diurnal changes, or salinity, less restrictive environmental conditions could allow for more LC-coacervate phases to assemble. Indeed, at a given peptide/DNA preparation, the LC-coacervate phase diagram crucially depends on temperature and salt concentration (Figure 3A). For example, LC-coacervate droplets can be found at 600 mM NaCl at 50 °C or 700 mM at 40 °C, while changes in temperature (vertical arrow in Figure 3A) and salinity (horizontal arrow in Figure 3A) result in direct transition between various mesophases. As a general behavior, the critical salt concentration, for coacervation or for each LC mesophase, decreases at increasing temperature (see magenta, blue, and red phase boundary lines in Figure 3A). This can be understood by considering that both salt and temperature regulate the non-covalent polymer/polymer interactions which determine the structure of the entire self-assembly. In the absence of (or presence of low concentrations of) salt or at low temperatures, some of the non-covalent interactions (primarily electrostatic interactions) between PLL and DNA are so strong that the PLL and DNA complex strongly in a fashion where precipitates form. However, a combination of both electrostatic and other non-covalent interactions (hydrogen bonding and stacking) are required to achieve both coacervation and LC formation. This can be achieved at specific salinities and temperatures, although at sufficiently high salinities and temperatures, disassembly would result due to screened electrostatic and disruption of all non-covalent interactions, respectively. Additional variations in peptide and DNA sequence and length could result in different ranges of salinities and temperatures required for LC-coacervate assembly, as commonly observed for isotropic coacervate assemblies [76]. Indeed, Archean ocean temperatures have been predicted to be much higher than the current ocean temperature (up to 70–80 °C) [87], although the exact value is under debate, as other simulations place the Archean climate in a more temperate range of up to 50 °C [88]. It is unclear what the exact salinity of the ancient ocean was, as studies have shown both saltier (by up to two-fold) [89] or similar salinity [90] ancient oceans compared to modern oceans. Different inland salty bodies of water, such as the Great Salt Lake [91,92] or the Dead Sea [93], have also been shown to have higher salinities than ocean water in addition to significant salinity variation within its different regions. This suggests that ancient ocean salinity may also have been variable depending on location. Water mixing regions, such as freshwater/saltwater mixed brackish regions [94] or even the boundary area between deep-sea brines (such as those found under the Red Sea [93,95]) and the ocean could have led to salinity gradients, resulting in accessibility to almost all possible salinities.

Thus, the uncertainty of the exact Archean ocean temperature and salinity, the possibility that ancient bodies of water varied in salinity depending on location, as well as the existence of water mixing areas suggest that there would likely have been some primitive environments with the correct temperature and salinity that could promote the assembly of LC-coacervate droplets. Salinity and temperature transitions caused by environmental effects (seasonal changes, precipitation, in-flow from freshwater bodies, etc.) or through transition between aquatic regions with different salinity or temperature could allow structural access to a significant part of a LC-coacervate phase diagram.

7. Stability-Based Evolutionary Scenarios in LC-Coacervate Systems

Environmental wet-dry and temperature cycles could have also been one way that selective pressure could be introduced to the system, eventually leading to improvements in stability, structure, and function of such phase-separated systems through chemical evolution on a structural scale, if not also on a polymer length and sequence scale (Figure 4). For instance, we can consider a system composed of peptides (with different length, sequence, and charge density) and anionic nucleic acid fragments

(with different length, sequence, structural motifs, and terminal interactions), either ssDNA/RNA or dsDNA/RNA, which can nucleate coacervates of different dimensions and stabilities, having different compositions (Figure 4A). T or [NaCl] variations result in a selection pressure, which results in the persistence of most stable compartments while the unstable ones disassemble (extinction events) and their constituents return to solution (Figure 4B). Upon cooling or dilution, the surviving coacervates can grow by incorporation of the dissociated and dissolved material in solution from the recently extinct droplets, resulting in formation of new (Figure 4C). Further T and salt increases will renew the selective pressure by generating new cycles of extinction and persistence (Figure 4D), eventually leading to the survival of only a few of the most stable compartments (Figure 4E); upon further reversal/variation of T or [NaCl], these droplets can further grow, this being a positive enrichment mechanism that rewards the selected individuals (Figure 4F). Further variations of the environmental conditions, eventually accompanied by the delivery (or formation) of new polymers and the degradation of others, would set the conditions for new selection rounds and conceivably lead to the evolution of the compartment population. Moreover, the formation of a functional compartment (such as the LC-coacervates) can itself modify the population of the available chemical species by favoring chemical modifications (such as ligation and polymerization [56–58]) which can lead to the further formation of longer polymers and new sequences, which in turn can further stabilize the compartment and sustain chemical evolution based on transient compartmentalization [96].
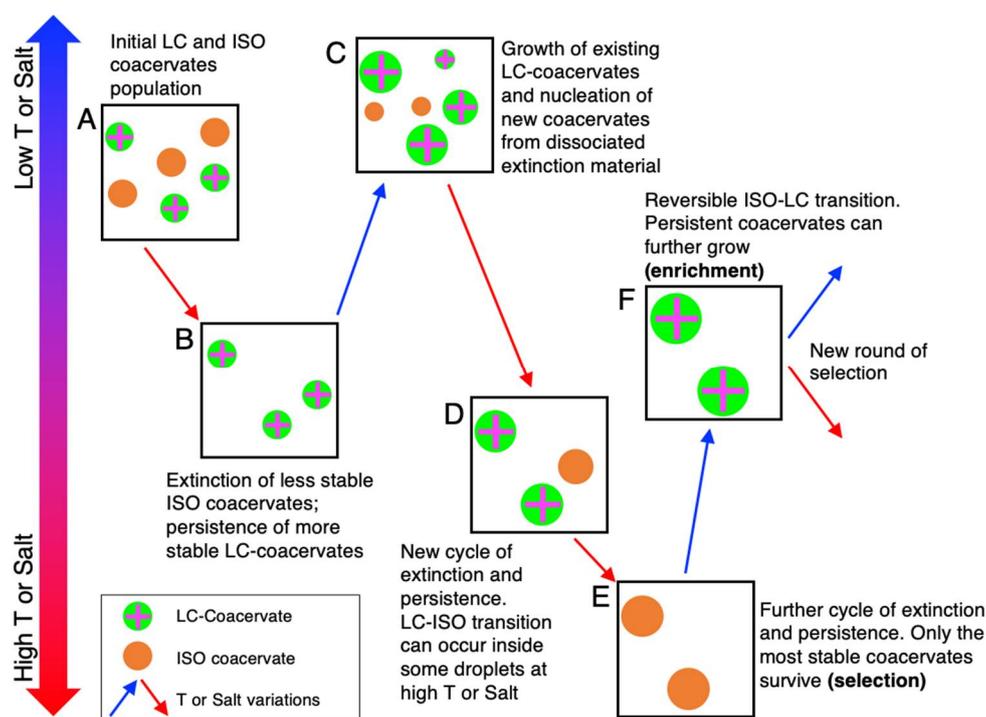

Figure 4. Selective evolution of LC-coacervates through variations in temperature, T, or salinity caused by environmental cycles. A mixed population of coacervates with different stabilities (due to peptide and/or DNA sequence differences) (**A**), which is reflected by the phase (LC or ISO) and/or to the dimension of the compartment, is subjected to increasing T or [NaCl] from dehydration, which results in extinction of the less stable ISO droplets and the persistence of the more stable LC droplets (**B**). Reversible cooling or hydration results in the potential growth of existing LC-coacervates as well as the nucleation of new coacervates (both LC and ISO) by recycling the dissociated material from the recently extinct droplets (**C**). Further heating or dehydration drives a further cycle of extinction and persistence (**D**), and even further heating will result in persistence of only the most stable coacervates

in the population (**E**). Eventually, LC–ISO transitions can occur within the droplets at increasing T. Finally, reversible cooling can result in the recovery and growth of the LC phase (ISO-LC transition), the latter being a positive enrichment mechanism (**F**). The whole process, which is based on a nucleation and growth process, will select compartments based on their stability and can be repeated for many rounds, resulting in the evolution of the initial population towards growing and persistent coacervates.

8. Relevance of Duplex DNA Structures over Single-Stranded DNA (ssDNA) Structures

The earliest genetic nucleic acid biopolymers (likely RNA) on Earth were likely single-strands which could synthesize their complementary strands through some form of template-directed synthesis [97]. However, once the complementary strand is synthesized, a nucleic acid duplex is formed, which cannot further polymerize or replicate without some mechanism to separate the two strands. Some proposed primitive mechanisms to achieve primitive post-polymerization strand separation include decrease of strand reannealing rate in viscous solvents after heat-separation of the duplex strands [98] and rapid pH oscillations in eutectic phases modulating the melting temperature of duplexes [99], however the exact mechanism has yet to be defined. DNA in modern organisms are generally completely in duplex form, other than when they are undergoing replication or transcription, where enzymes such as helicases, which unwind the dsDNA into separate single strands, allow such dsDNA to undergo template-directed polymerization processes [100]. Clearly, a dsDNA structure was chosen by evolution as the preferred nucleic acid architecture over single strands despite the necessity of evolving specific enzymes whose main role is to separate such duplex strands.

Aside from greater stability of hydrolysis of duplexes vs. single strands [101], or a duplex containing a "backup" copy of genetic information as a way to prevent loss of information errors in case of mutation or deletion (such as through error correction enzymes) [102], there may be further structural reasons, relevant to some of the observations presented about the LC-coacervate system studied herein, that resulted in evolution from ssDNA to dsDNA. For example, stiffer duplex nucleic acid structures allow accession of further structural diversity and complexity, such as in the form of LCs, than flexible single strands which prefer globular conformations and cannot access LC phases. Of course, increased structural diversity and complexity does not necessarily guarantee a selective advantage, but studies in the biotechnology field have revealed potentially prebiotically relevant (and advantageous) functions. As LC phases have been used in applications such as cell culture scaffolds [103], an LC phase coupled to a primitive compartment (such as that of a membraneless phase-separated droplet, which has now been shown to readily assembly under dsDNA conditions as well as the previously well-studied ssDNA conditions [104]) could allow the scaffolding of complex functional 3D assemblies composed of other biomolecules such as other peptides or amino acids. Such LC scaffolds could also promote optimal spatial organization for a growing droplet system, while potentially regulating protocell–protocell interactions. An LC exterior could also change the electrochemical properties of such compartments, providing greater mass and charge transfer that could be essential for catalysis of compartmentalized redox reactions [52], reaction types that are heavily implied to be necessary during the origins of life [105]. It has also been shown that LCs can control the stereoselectivity or regioselectivity of certain reaction products [51], suggesting one further mechanism by which a simple coacervate compartment could effect primitive selective reaction control.

Finally, within an LC-coacervate system, dsDNA is in a linear conformation (a requirement of LC phase assembly), whereas ssDNA in an ISO coacervate system would likely be in a disordered, non-linear conformation [63]. As it has been shown that nucleic acid ligation is critically enhanced when linear reversible aggregation of end-to-end interacting duplexes is sustained by LC ordering which keeps the duplexes in close contact [56], more efficient ligation of the nucleic acid components of an LC-containing compartment system could result in longer, and more diverse, nucleic acid products, contributing to enhanced evolutionary efficiency and efficacy. Additionally, dsRNA-based LC structures have been characterized [58,106], which suggests that it may be possible for a primitive linear dsRNA LC-coacervate system, which would be similar in structure and properties

to the current dsDNA LC-coacervate system, containing a functional RNA ribozyme to also have assembled before (or concurrently with) the advent of DNA. The interior of the LC-coacervate droplet is molecularly crowded and contains a high concentration of peptide, which itself may also be guided in a linear confirmation due binding with the linear nucleic acid components. Such peptide-nucleic acid binding and molecular crowding [107] could have promoted accession and evolution of different (and/or more functional) ribozyme functions, potentially leading to co-evolution of primitive ribo-nucleo-peptides [108,109]. Remarkably, LC ordering can even take place in mixtures of complementary nucleotides [40], whose pairing and stacking are stabilized by the entire phase self-assembly. This suggests that in principle the coupling of LC-coacervation of single nucleotides and enhanced polymerization could provide a pathway for the prebiotic emergence of the first nucleic acid polymers.

9. Conclusions

In the context of origins of life, membraneless coacervate systems have been proposed to be one model primitive compartment system [110]. One major challenge in our current understanding of primitive compartments is how such compartments can increase in structural, genetic, and catalytic complexity, as a means to sustain further chemical evolution. In this frame, a nucleic acid-peptide LC-coacervate system could simultaneously: (i) increase the structural complexity of the system through assembly of supramolecular long-range-ordered but still fluid phases; (ii) concentrate, select, and protect nucleic acids within a compartment; and (iii) increase the compartment's stability to fluctuations in temperature and salt concentration. In fact, the entire known LC mesophase space can be accessed through mild temperature and hydration cycles [23] resulting from geological processes such as seasonal, precipitation, or diurnal cycles. This observation suggests that not only could a primitive LC-coacervate system more effectively survive and reassemble upon environmental cycles on early Earth, but such cycles (for example, wet–drying cycles on a coastal oceanic or inland sea environment [111]) could have been essential to enable compartment selection based on a nucleation and growth process, in turn sustaining structural and compositional evolution of a primitive LC-coacervate population towards a more stable configuration. Wet–dry cycles, while possibly promoting initial oligomeric nucleic acid and peptide polymerization from monomeric building blocks, could also serve to activate or inactivate functional LC-coacervate structures, which in turn can enhance the polymerization efficacy of long linear nucleic acids and peptides. In this view, chemical evolution of the molecular species would be connected with a positive feedback loop of stability-based evolution of the compartments.

10. Methods

Chemicals. DNA rDD (5′-GCGCTTAAGCGC-3′) was synthesized internally with an Akta-Oligopilot (GE Healthcare Life Sciences, Marlborough, MA, USA), followed by high-performance liquid chromatography (HPLC) purification (Varian Prostar 218 system, Varian, Palo Alto, CA, USA). This procedure is described by Bellini et al. [38]. For further preparation, rDD was dialyzed against 1 L of 10 mM NaCl for 48 h, with dialysis buffer replacement after 2, 4, and 12 h. After this, rDD was subsequently lyophilized. All other chemicals, including PLL (poly-L-lysine hydrobromide 30 kDa–70 kDa, P2636), were purchased from Sigma-Aldrich, Inc. (St. Louis, MI, USA) unless otherwise indicated. All solutions were prepared in MilliQ water, Millipore (Burlington, MA, USA).

Sample preparation and microscopy. LC-coacervate sample preparation and analysis was performed in a similar fashion to that reported previously by Fraccia and Jia [63].

We first prepared stock solutions of rDD and PLL of 100 mM total charge (P = 100 mM or N = 100 mM, respectively). A 2 M NaCl stock solution was also prepared. In a plastic 0.2 mL microcentrifuge tube (Eppendorf, Hamburg, Germany), stock solutions were mixed at room temperature to prepare a 10 μL sample containing rDD (P = 10 mM), PLL (N = 10 mM), and NaCl (at varying concentrations). NaCl was always added first, followed by PLL and then rDD, to avoid precipitation.

Annealing was performed in columnar samples (Figure 1), which consisted of heating the sample to 95 °C for 10 min followed by cooling to room temperature slowly ($\Delta T/t \leq 5$ °C/min) on a polymerase chain reaction (PCR) thermocycler (Eppendorf, Hamburg, Germany) or directly on the microscope heating stage (see below for specifications). SYBR Gold (Thermo-Fisher, Waltham, MA, USA) was added to certain samples (Figure 2) at a 1:10000× ratio at room temperature.

Then, 10 µL of each prepared rDD-PLL solution was transferred to the bottom of a 384 well microplate with either a non-binding surface polystyrene (code 3544) or glass bottom (code 4581) (Corning, New York, USA), the latter previously passivated with 3.5% bovine serum albumin solution, followed by addition of 40 µL of "light" mineral oil (M5904, Sigma-Aldrich) and application of plastic PCR film (Bio-rad, Segrate, Italy) to prevent evaporation (this step was omitted for experiments concerning wet-dry cycling). Fluorescence (FITC filter cube), BFTOM, and PTOM microscopy images were acquired with a Nikon (Shinagawa-ku, Tokyo, Japan) Ti-U inverted fluorescent microscope equipped with linear polarizer and analyzer on a 20× air objective or a Leica (Wetzlar, Germany) DMi8 confocal microscope. Temperature was controlled with an Instec (Boulder, Colorado, USA) TSA12Gi peltier hot/cold stage. Observation was undertaken after at least 10 min incubation time, to allow each phase to reach equilibrium. Dehydration for certain experiments was performed by simply allowing the water in the sample well to evaporate at room temperature while gently flushing dry compressed air on the sample (to speed up the evaporation process).

All images were analyzed using FIJI (Fiji is Just ImageJ, http://fiji.sc). Particle size and total volume occupied by the coacervate phase was calculated by using the "Particle Analysis" function of ImageJ. The area of all individual droplets was estimated, excluding those that touched an edge and those with small measured areas (10 pixels or less) which likely represented fluorescence saturation. Almost all of the droplets were circular, so a "Circularity Filter" was not used. Then, the average area as well as the total area at each data point were computed using the complete list of individual droplet areas.

DNA Concentration Calculations. DNA concentration calculations were performed in a method identical to a previous study [63].

Briefly, an indirect method to measure DNA concentration within the LC-coacervate droplets was utilized due to the low amount of material available. After formation of the charge-balanced (N = P = 10 mM) LC-coacervates (at 600 mM, 700 mM, 800 mM, and 900 mM NaCl), the samples were centrifuged for 10 min at 5000 rcf, followed by extraction and dilution of 5 µL of the supernatant phase in 20 µL 1M NaCl; this step ensures that all rDD-PLL complexes in the supernatant are disassociated. The DNA concentration in the supernatant was then measured through its ultraviolet (UV) absorbance at 260 nm through a Nanodrop One UV–Vis (ultraviolet–visible) spectrophotometer (Thermo-Fisher Scientific, Waltham, MA, USA). Conversion from absorbance to concentration was performed using a theoretical extinction coefficient for double stranded rDD (ε_{rDD} = 199,349 mol^{-1}cm^{-1}). Each sample was prepared in duplicate, and the measurements were performed in triplicate.

Next, to estimate the concentration of rDD within the droplets, the volume fraction of the dense coacervate phase (the volume occupied by the coacervate phase divided by the total volume) was first estimated through confocal microscopy images of LC-coacervates (containing a 1:1000 PLL-FITC (fluorescein isothiocyanate-labeled poly-L-lysine 30 kDa–70 kDa)) acquired in a previous study [63] (Leica (Wetzlar, Germany) SP8 confocal fluorescence microscope using a 20× objective (N.A.: 0.75) with or green (488 nm) laser excitation (diode laser)). The volume fraction was obtained by adding the volumes of the droplets in a field of view (258.33 µm × 258.33 µm, corresponding to 1960 pix × 1960 pix), specifically chosen near the bottom of the well as we assumed that most of the droplets resided near the bottom after an incubation time, divided by the volume of the parallelepiped occupied by the sample, (with a height of 796 µm, which was estimated from the fact that the 10 µL solution filled a cylindrical well in a 384 multi-well plate with well-diameter of 4 mm; we assumed that the liquid volume was a cylinder, despite the likelihood of a meniscus at the top of the sample well, for ease of calculation and due to the fact that measurements were performed at different locations in the well). The volume occupied by the droplets was calculated through the ImageJ "Particle Analysis"

function by estimating the area occupied by each particle (we excluded particles touching an edge, and particles with measured areas less than 10 pixels). A circularity filter was not applied, and the area was converted to a radius, and then a volume for each particle; we assumed that each particle was a perfect sphere for ease of calculation, and measurements were averaged over three different fields of view to account for potential sample inhomogeneities.

Finally, the concentration of DNA in the droplets was obtained as the total DNA in the droplets plus the total DNA outside of the droplets must be equivalent to the total amount of DNA introduced into the entire sample initially. That is to say that the (DNA concentration in the droplets) * (volume fraction of the coacervate phase) + (DNA concentration outside of the droplets) * (volume fraction of the supernatant phase) = the total DNA introduced (10 μL sample of 0.91 mM DNA).

References

1. Szostak, J.W.; Bartel, D.P.; Luigi Luisi, P. Synthesizing life. *Nature* **2001**, *409*, 387–390. [CrossRef] [PubMed]

2. Bansho, Y.; Furubayashi, T.; Ichihashi, N.; Yomo, T. Host–parasite oscillation dynamics and evolution in a compartmentalized RNA replication system. *Proc. Natl. Acad. Sci. USA* **2016**, *113*, 4045–4050. [CrossRef] [PubMed]

3. Chen, I.A.; Walde, P. From self-assembled vesicles to protocells. *Cold Spring Harb. Perspect. Biol.* **2010**, *2*, a002170. [CrossRef] [PubMed]

4. Wang, L.; Song, S.; van Hest, J.; Abdelmohsen, L.K.E.A.; Huang, X.; Sánchez, S. Biomimicry of Cellular Motility and Communication Based on Synthetic Soft-Architectures. *Small* **2020**, *16*, e1907680. [CrossRef] [PubMed]

5. Dzieciol, A.J.; Mann, S. Designs for life: Protocell models in the laboratory. *Chem. Soc. Rev.* **2012**, *41*, 79–85. [CrossRef] [PubMed]

6. Yoshizawa, T.; Nozawa, R.-S.; Jia, T.Z.; Saio, T.; Mori, E. Biological phase separation: Cell biology meets biophysics. *Biophys. Rev.* **2020**, *12*, 519–539. [CrossRef] [PubMed]

7. Shin, Y.; Brangwynne, C.P. Liquid phase condensation in cell physiology and disease. *Science* **2017**, *357*, eaaf4382. [CrossRef]

8. Keating, C.D. Aqueous phase separation as a possible route to compartmentalization of biological molecules. *Acc. Chem. Res.* **2012**, *45*, 2114–2124. [CrossRef]

9. Mann, S. Systems of Creation: The Emergence of Life from Nonliving Matter. *Acc. Chem. Res.* **2012**, *45*, 2131–2141. [CrossRef]

10. Nakashima, K.K.; Vibhute, M.A.; Spruijt, E. Biomolecular Chemistry in Liquid Phase Separated Compartments. *Front. Mol. Biosci.* **2019**, *6*, 21. [CrossRef]

11. Sing, C.E.; Perry, S.L. Recent progress in the science of complex coacervation. *Soft Matter* **2020**, *16*, 2885–2914. [CrossRef] [PubMed]

12. Aumiller, W.M., Jr.; Pir Cakmak, F.; Davis, B.W.; Keating, C.D. RNA-Based Coacervates as a Model for Membraneless Organelles: Formation, Properties, and Interfacial Liposome Assembly. *Langmuir* **2016**, *32*, 10042–10053. [CrossRef]

13. Jia, T.Z.; Hentrich, C.; Szostak, J.W. Rapid RNA Exchange in Aqueous Two-Phase System and Coacervate Droplets. *Orig. Life Evol. Biosph.* **2014**, *44*, 1–12. [CrossRef]

14. Koga, S.; Williams, D.S.; Perriman, A.W.; Mann, S. Peptide-nucleotide microdroplets as a step towards a membrane-free protocell model. *Nat. Chem.* **2011**, *3*, 720–724. [CrossRef]

15. Jia, T.Z.; Chandru, K.; Hongo, Y.; Afrin, R.; Usui, T.; Myojo, K.; Cleaves, H.J., 2nd. Membraneless polyester microdroplets as primordial compartments at the origins of life. *Proc. Natl. Acad. Sci. USA* **2019**, *116*, 15830–15835. [CrossRef]

16. Frankel, E.A.; Bevilacqua, P.C.; Keating, C.D. Polyamine/Nucleotide Coacervates Provide Strong Compartmentalization of Mg^{2+}, Nucleotides, and RNA. *Langmuir* **2016**, *32*, 2041–2049. [CrossRef] [PubMed]

17. Tang, T.-Y.D.; Rohaida Che Hak, C.; Thompson, A.J.; Kuimova, M.K.; Williams, D.S.; Perriman, A.W.; Mann, S. Fatty acid membrane assembly on coacervate microdroplets as a step towards a hybrid protocell model. *Nat. Chem.* **2014**, *6*, 527–533. [CrossRef] [PubMed]

18. Drobot, B.; Iglesias-Artola, J.M.; Le Vay, K.; Mayr, V.; Kar, M.; Kreysing, M.; Mutschler, H.; Tang, T.-Y.D. Compartmentalised RNA catalysis in membrane-free coacervate protocells. *Nat. Commun.* **2018**, *9*, 3643. [CrossRef]

19. Poudyal, R.R.; Guth-Metzler, R.M.; Veenis, A.J.; Frankel, E.A.; Keating, C.D.; Bevilacqua, P.C. Template-directed RNA polymerization and enhanced ribozyme catalysis inside membraneless compartments formed by coacervates. *Nat. Commun.* **2019**, *10*, 490. [CrossRef]

20. Perry, S.L.; Leon, L.; Hoffmann, K.Q.; Kade, M.J.; Priftis, D.; Black, K.A.; Wong, D.; Klein, R.A.; Pierce, C.F., 3rd; Margossian, K.O.; et al. Chirality-selected phase behaviour in ionic polypeptide complexes. *Nat. Commun.* **2015**, *6*, 6052. [CrossRef]

21. Perry, S.; Li, Y.; Priftis, D.; Leon, L.; Tirrell, M. The Effect of Salt on the Complex Coacervation of Vinyl Polyelectrolytes. *Polymers* **2014**, *6*, 1756–1772. [CrossRef]

22. Priftis, D.; Tirrell, M. Phase behaviour and complex coacervation of aqueous polypeptide solutions. *Soft Matter* **2012**, *8*, 9396–9405. [CrossRef]

23. Mulkidjanian, A.Y.; Bychkov, A.Y.; Dibrova, D.V.; Galperin, M.Y.; Koonin, E.V. Origin of first cells at terrestrial, anoxic geothermal fields. *Proc. Natl. Acad. Sci. USA* **2012**, *109*, E821–E830. [CrossRef]

24. Fares, H.; Marras, A.; Ting, J.; Tirrell, M.; Keating, C. Impact of Wet-Dry Cycling on the Phase Behavior and Compartmentalization Properties of Complex Coacervates. *ChemRXiv* **2020**. [CrossRef]

25. Parker, E.T.; Cleaves, H.J.; Dworkin, J.P.; Glavin, D.P.; Callahan, M.; Aubrey, A.; Lazcano, A.; Bada, J.L. Primordial synthesis of amines and amino acids in a 1958 Miller H_2S-rich spark discharge experiment. *Proc. Natl. Acad. Sci. USA* **2011**, *108*, 5526–5531. [CrossRef]

26. Koga, T.; Naraoka, H. A new family of extraterrestrial amino acids in the Murchison meteorite. *Sci. Rep.* **2017**, *7*, 636. [CrossRef] [PubMed]

27. Orgel, L.E. Polymerization on the rocks: Theoretical introduction. *Orig. Life Evol. Biosph.* **1998**, *28*, 227–234. [CrossRef] [PubMed]

28. Forsythe, J.G.; Yu, S.-S.; Mamajanov, I.; Grover, M.A.; Krishnamurthy, R.; Fernández, F.M.; Hud, N.V. Ester-Mediated Amide Bond Formation Driven by Wet-Dry Cycles: A Possible Path to Polypeptides on the Prebiotic Earth. *Angew. Chem. Int. Ed Engl.* **2015**, *54*, 9871–9875. [CrossRef]

29. Furukawa, Y.; Chikaraishi, Y.; Ohkouchi, N.; Ogawa, N.O.; Glavin, D.P.; Dworkin, J.P.; Abe, C.; Nakamura, T. Extraterrestrial ribose and other sugars in primitive meteorites. *Proc. Natl. Acad. Sci. USA* **2019**, *116*, 24440–24445. [CrossRef]

30. Becker, S.; Feldmann, J.; Wiedemann, S.; Okamura, H.; Schneider, C.; Iwan, K.; Crisp, A.; Rossa, M.; Amatov, T.; Carell, T. Unified prebiotically plausible synthesis of pyrimidine and purine RNA ribonucleotides. *Science* **2019**, *366*, 76–82. [CrossRef]

31. Higgs, P.G. The Effect of Limited Diffusion and Wet-Dry Cycling on Reversible Polymerization Reactions: Implications for Prebiotic Synthesis of Nucleic Acids. *Life* **2016**, *6*, 24. [CrossRef]

32. Szostak, J.W. The Narrow Road to the Deep Past: In Search of the Chemistry of the Origin of Life. *Angew. Chem. Int. Ed. Engl.* **2017**, *56*, 11037–11043. [CrossRef] [PubMed]

33. Gilbert, W. Origin of life: The RNA world. *Nature* **1986**, *319*, 618. [CrossRef]

34. Bhowmik, S.; Krishnamurthy, R. The role of sugar-backbone heterogeneity and chimeras in the simultaneous emergence of RNA and DNA. *Nat. Chem.* **2019**, *11*, 1009–1018. [CrossRef]

35. Hong, F.; Zhang, F.; Liu, Y.; Yan, H. DNA Origami: Scaffolds for Creating Higher Order Structures. *Chem. Rev.* **2017**, *117*, 12584–12640. [CrossRef]

36. Han, D.; Qi, X.; Myhrvold, C.; Wang, B.; Dai, M.; Jiang, S.; Bates, M.; Liu, Y.; An, B.; Zhang, F.; et al. Single-stranded DNA and RNA origami. *Science* **2017**, *358*, eaao2648. [CrossRef]

37. Anastassacos, F.M.; Zhao, Z.; Zeng, Y.; Shih, W.M. Glutaraldehyde Cross-Linking of Oligolysines Coating DNA Origami Greatly Reduces Susceptibility to Nuclease Degradation. *J. Am. Chem. Soc.* **2020**, *142*, 3311–3315. [CrossRef]

38. Bellini, T.; Zanchetta, G.; Fraccia, T.P.; Cerbino, R.; Tsai, E.; Smith, G.P.; Moran, M.J.; Walba, D.M.; Clark, N.A. Liquid crystal self-assembly of random-sequence DNA oligomers. *Proc. Natl. Acad. Sci. USA* **2012**, *109*, 1110–1115. [CrossRef]

39. Fraccia, T.P.; Smith, G.P.; Bethge, L.; Zanchetta, G.; Nava, G.; Klussmann, S.; Clark, N.A.; Bellini, T. Liquid Crystal Ordering and Isotropic Gelation in Solutions of Four-Base-Long DNA Oligomers. *ACS Nano* **2016**, *10*, 8508–8516. [CrossRef] [PubMed]

40. Smith, G.P.; Fraccia, T.P.; Todisco, M.; Zanchetta, G.; Zhu, C.; Hayden, E.; Bellini, T.; Clark, N.A. Backbone-free duplex-stacked monomer nucleic acids exhibiting Watson-Crick selectivity. *Proc. Natl. Acad. Sci. USA* **2018**, *115*, E7658–E7664. [CrossRef] [PubMed]

41. Sakurai, S.; Jo, K.; Kinoshita, H.; Esumi, M.; Tanaka, M. Guanine damage by singlet oxygen from SYBR Green I in liquid crystalline DNA. *Org. Biomol. Chem.* **2020**. [CrossRef]

42. Livolant, F.; Levelut, A.M.; Doucet, J.; Benoit, J.P. The highly concentrated liquid-crystalline phase of DNA is columnar hexagonal. *Nature* **1989**, *339*, 724–726. [CrossRef]

43. Nakata, M.; Zanchetta, G.; Chapman, B.D.; Jones, C.D.; Cross, J.O.; Pindak, R.; Bellini, T.; Clark, N.A. End-to-end stacking and liquid crystal condensation of 6 to 20 base pair DNA duplexes. *Science* **2007**, *318*, 1276–1279. [CrossRef] [PubMed]

44. Zanchetta, G.; Bellini, T.; Nakata, M.; Clark, N.A. Physical polymerization and liquid crystallization of RNA oligomers. *J. Am. Chem. Soc.* **2008**, *130*, 12864–12865. [CrossRef]

45. Di Leo, S.; Todisco, M.; Bellini, T.; Fraccia, T.P. Phase separations, liquid crystal ordering and molecular partitioning in mixtures of PEG and DNA oligomers. *Liq. Cryst.* **2018**, *45*, 2306–2318. [CrossRef]

46. Fraccia, T.; Smith, G.; Clark, N.; Bellini, T. Liquid Crystal Ordering of Four-Base-Long DNA Oligomers with Both G–C and A–T Pairing. *Crystals* **2017**, *8*, 5. [CrossRef]

47. Leforestier, A.; Livolant, F. The bacteriophage genome undergoes a succession of intracapsid phase transitions upon DNA ejection. *J. Mol. Biol.* **2010**, *396*, 384–395. [CrossRef]

48. Manning, G.S. The persistence length of DNA is reached from the persistence length of its null isomer through an internal electrostatic stretching force. *Biophys. J.* **2006**, *91*, 3607–3616. [CrossRef] [PubMed]

49. Matczyszyn, K.; Olesiak-Banska, J. DNA as scaffolding for nanophotonic structures. *J. Nanophotonics* **2012**, *6*, 064505. [CrossRef]

50. Sung, B.; Kim, M.-H. Liquid-crystalline nanoarchitectures for tissue engineering. *Beilstein J. Nanotechnol.* **2018**, *9*, 205–215. [CrossRef]

51. Kansui, H.; Hiraoka, S.; Kunieda, T. Liquid Crystal Control of Bimolecular Thermal Reactions. Highly Regioselective Pericycloaddition of Fumarates to 2,6-Dialkoxyanthracenes in Liquid−Crystalline Media. *J. Am. Chem. Soc.* **1996**, *118*, 5346–5352. [CrossRef]

52. Rusling, J.F. Liquid crystal surfactant films for electrochemical catalysis. *Microporous Mater.* **1994**, *3*, 1–16. [CrossRef]

53. Lucchetti, L.; Fraccia, T.P.; Ciciulla, F.; Bellini, T. Non-linear optical measurement of the twist elastic constant in thermotropic and DNA lyotropic chiral nematics. *Sci. Rep.* **2017**, *7*, 4959. [CrossRef] [PubMed]

54. Lucchetti, L.; Fraccia, T.P.; Ciciulla, F.; Simoni, F.; Bellini, T. Giant optical nonlinearity in DNA lyotropic liquid crystals. *Opt. Express* **2017**, *25*, 25951–25959. [CrossRef]

55. Lucchetti, L.; Fraccia, T.P.; Nava, G.; Turiv, T.; Ciciulla, F.; Bethge, L.; Klussmann, S.; Lavrentovich, O.D.; Bellini, T. Elasticity and Viscosity of DNA Liquid Crystals. *ACS Macro Lett.* **2020**, *9*, 1034–1039. [CrossRef]

56.   Fraccia, T.P.; Smith, G.P.; Zanchetta, G.; Paraboschi, E.; Yi, Y.; Walba, D.M.; Dieci, G.; Clark, N.A.; Bellini, T. Abiotic ligation of DNA oligomers templated by their liquid crystal ordering. *Nat. Commun.* **2015**, *6*, 6424. [CrossRef]

57.   Fraccia, T.P.; Zanchetta, G.; Rimoldi, V.; Clark, N.A.; Bellini, T. Evidence of Liquid Crystal–Assisted Abiotic Ligation of Nucleic Acids. *Orig. Life Evol. Biosph.* **2015**, *45*, 51–68. [CrossRef]

58.   Todisco, M.; Fraccia, T.P.; Smith, G.P.; Corno, A.; Bethge, L.; Klussmann, S.; Paraboschi, E.M.; Asselta, R.; Colombo, D.; Zanchetta, G.; et al. Nonenzymatic Polymerization into Long Linear RNA Templated by Liquid Crystal Self-Assembly. *ACS Nano* **2018**, *12*, 9750–9762. [CrossRef]

59.   Mountain, G.A.; Keating, C.D. Formation of Multiphase Complex Coacervates and Partitioning of Biomolecules within them. *Biomacromolecules* **2019**, *21*, 630–640. [CrossRef]

60.   Lu, T.; Spruijt, E. Multiphase Complex Coacervate Droplets. *J. Am. Chem. Soc.* **2020**, *142*, 2905–2914. [CrossRef]

61.   Sato, Y.; Sakamoto, T.; Takinoue, M. Sequence-based engineering of dynamic functions of micrometer-sized DNA droplets. *Sci. Adv.* **2020**, *6*, eaba3471. [CrossRef] [PubMed]

62.   Rumyantsev, A.M.; de Pablo, J.J. Liquid Crystalline and Isotropic Coacervates of Semiflexible Polyanions and Flexible Polycations. *Macromolecules* **2019**, *52*, 5140–5156. [CrossRef]

63.   Fraccia, T.P.; Jia, T.Z. Liquid Crystal Coacervates Composed of Short Double-Stranded DNA and Cationic Peptides. *ACS Nano* **2020**. [CrossRef] [PubMed]

64.   Shakya, A.; King, J.T. DNA Local-Flexibility-Dependent Assembly of Phase-Separated Liquid Droplets. *Biophys. J.* **2018**, *115*, 1840–1847. [CrossRef] [PubMed]

65.   Priftis, D.; Megley, K.; Laugel, N.; Tirrell, M. Complex coacervation of poly(ethylene-imine)/polypeptide aqueous solutions: Thermodynamic and rheological characterization. *J. Colloid Interface Sci.* **2013**, *398*, 39–50. [CrossRef] [PubMed]

66.   Pearce, B.K.D.; Pudritz, R.E.; Semenov, D.A.; Henning, T.K. Origin of the RNA world: The fate of nucleobases in warm little ponds. *Proc. Natl. Acad. Sci. USA* **2017**, *114*, 11327–11332. [CrossRef]

67.   Todisco, M.; Smith, G.P.; Fraccia, T.P. Liquid Crystal ordering of DNA Dickerson Dodecamer duplexes with different 5'- Phosphate terminations. *Mol. Cryst. Liq. Cryst.* **2019**, *683*, 69–80. [CrossRef]

68.   Livolant, F.; Maestre, M.F. Circular dichroism microscopy of compact forms of DNA and chromatin in vivo and in vitro: Cholesteric liquid-crystalline phases of DNA and single dinoflagellate nuclei. *Biochemistry* **1988**, *27*, 3056–3068. [CrossRef]

69.   Owczarzy, R.; You, Y.; Moreira, B.G.; Manthey, J.A.; Huang, L.; Behlke, M.A.; Walder, J.A. Effects of sodium ions on DNA duplex oligomers: Improved predictions of melting temperatures. *Biochemistry* **2004**, *43*, 3537–3554. [CrossRef]

70.   Kreysing, M.; Keil, L.; Lanzmich, S.; Braun, D. Heat flux across an open pore enables the continuous replication and selection of oligonucleotides towards increasing length. *Nat. Chem.* **2015**, *7*, 203–208. [CrossRef]

71.   Mullineaux, L.S.; Metaxas, A.; Beaulieu, S.E.; Bright, M.; Gollner, S.; Grupe, B.M.; Herrera, S.; Kellner, J.B.; Levin, L.A.; Mitarai, S.; et al. Exploring the Ecology of Deep-Sea Hydrothermal Vents in a Metacommunity Framework. *Front. Mar. Sci.* **2018**, *5*, 1158. [CrossRef]

72.   Fu, J.; Schlenoff, J.B. Driving Forces for Oppositely Charged Polyion Association in Aqueous Solutions: Enthalpic, Entropic, but Not Electrostatic. *J. Am. Chem. Soc.* **2016**, *138*, 980–990. [CrossRef] [PubMed]

73.   Kilchherr, F.; Wachauf, C.; Pelz, B.; Rief, M.; Zacharias, M.; Dietz, H. Single-molecule dissection of stacking forces in DNA. *Science* **2016**, *353*. [CrossRef] [PubMed]

74.   SantaLucia, J., Jr.; Hicks, D. The thermodynamics of DNA structural motifs. *Annu. Rev. Biophys. Biomol. Struct.* **2004**, *33*, 415–440. [CrossRef]

75.   Elder, R.M.; Emrick, T.; Jayaraman, A. Understanding the effect of polylysine architecture on DNA binding using molecular dynamics simulations. *Biomacromolecules* **2011**, *12*, 3870–3879. [CrossRef]

76.   Vieregg, J.R.; Lueckheide, M.; Marciel, A.B.; Leon, L.; Bologna, A.J.; Rivera, J.R.; Tirrell, M.V. Oligonucleotide-Peptide Complexes: Phase Control by Hybridization. *J. Am. Chem. Soc.* **2018**, *140*, 1632–1638. [CrossRef]

77.   Zouhir, S.; Perchat, S.; Nicaise, M.; Perez, J.; Guimaraes, B.; Lereclus, D.; Nessler, S. Peptide-binding dependent conformational changes regulate the transcriptional activity of the quorum-sensor NprR. *Nucleic Acids Res.* **2013**, *41*, 7920–7933. [CrossRef]

78. Upadhyay, S.K. Binding and thermodynamics of REV peptide-ctDNA interaction. *Biopolymers* **2017**, *108*, e22902. [CrossRef]

79. Solovyev, A.Y.; Tarnovskaya, S.I.; Chernova, I.A.; Shataeva, L.K.; Skorik, Y.A. The interaction of amino acids, peptides, and proteins with DNA. *Int. J. Biol. Macromol.* **2015**, *78*, 39–45. [CrossRef]

80. Ross, D.S.; Deamer, D. Dry/Wet Cycling and the Thermodynamics and Kinetics of Prebiotic Polymer Synthesis. *Life* **2016**, *6*, 28. [CrossRef]

81. Campbell, T.D.; Febrian, R.; McCarthy, J.T.; Kleinschmidt, H.E.; Forsythe, J.G.; Bracher, P.J. Prebiotic condensation through wet-dry cycling regulated by deliquescence. *Nat. Commun.* **2019**, *10*, 4508. [CrossRef]

82. Chandru, K.; Guttenberg, N.; Giri, C.; Hongo, Y.; Butch, C.; Mamajanov, I.; James Cleaves, H. Simple prebiotic synthesis of high diversity dynamic combinatorial polyester libraries. *Commun. Chem.* **2018**, *1*, 30. [CrossRef]

83. Mamajanov, I.; MacDonald, P.J.; Ying, J.; Duncanson, D.M.; Dowdy, G.R.; Walker, C.A.; Engelhart, A.E.; Fernández, F.M.; Grover, M.A.; Hud, N.V.; et al. Ester Formation and Hydrolysis during Wet–Dry Cycles: Generation of Far-from-Equilibrium Polymers in a Model Prebiotic Reaction. *Macromolecules* **2014**, *47*, 1334–1343. [CrossRef]

84. Becker, S.; Schneider, C.; Okamura, H.; Crisp, A.; Amatov, T.; Dejmek, M.; Carell, T. Wet-dry cycles enable the parallel origin of canonical and non-canonical nucleosides by continuous synthesis. *Nat. Commun.* **2018**, *9*, 163. [CrossRef]

85. Hud, N.V. Searching for lost nucleotides of the pre-RNA World with a self-refining model of early Earth. *Nat. Commun.* **2018**, *9*, 5171. [CrossRef] [PubMed]

86. Li, D.; Liu, S. Seawater Quality Detection. In *Water Quality Monitoring and Management*; Elsevier: Amsterdam, The Netherlands, 2019; pp. 233–249. ISBN 9780128113301.

87. Garcia, A.K.; Schopf, J.W.; Yokobori, S.-I.; Akanuma, S.; Yamagishi, A. Reconstructed ancestral enzymes suggest long-term cooling of Earth's photic zone since the Archean. *Proc. Natl. Acad. Sci. USA* **2017**, *114*, 4619–4624. [CrossRef]

88. Krissansen-Totton, J.; Arney, G.N.; Catling, D.C. Constraining the climate and ocean pH of the early Earth with a geological carbon cycle model. *Proc. Natl. Acad. Sci. USA* **2018**, *115*, 4105–4110. [CrossRef] [PubMed]

89. Knauth, L.P. Temperature and salinity history of the Precambrian ocean: Implications for the course of microbial evolution. In *Geobiology: Objectives, Concepts, Perspectives*; Elsevier: Amsterdam, The Netherlands, 2005; pp. 53–69. ISBN 9780444520197.

90. Marty, B.; Avice, G.; Bekaert, D.V.; Broadley, M.W. Salinity of the Archaean oceans from analysis of fluid inclusions in quartz. *C. R. Geosci.* **2018**, *350*, 154–163. [CrossRef]

91. Stephens, D.W. Changes in lake levels, salinity and the biological community of Great Salt Lake (Utah, USA), 1847–1987. In *Saline Lakes*; Comín, F.A., Northcote, T.G., Eds.; Utah Geological and Mineral Survey Bull; Springer: Dordrecht, The Netherlands, 1990; Volume 913, pp. 139–146. ISBN 9789401067591.

92. Baxter, B.K. Great Salt Lake microbiology: A historical perspective. *Int. Microbiol.* **2018**, *21*, 79–95. [CrossRef]

93. Lensky, N.G.; Dvorkin, Y.; Lyakhovsky, V.; Gertman, I.; Gavrieli, I. Water, salt, and energy balances of the Dead Sea: MASS AND ENERGY BALANCES OF THE DEAD SEA. *Water Resour. Res.* **2005**, *41*, 513. [CrossRef]

94. Obolewski, K.; Glińska-Lewczuk, K.; Szymańska, M.; Mrozińska, N.; Bąkowska, M.; Astel, A.; Lew, S.; Paturej, E. Patterns of salinity regime in coastal lakes based on structure of benthic invertebrates. *PLoS ONE* **2018**, *13*, e0207825. [CrossRef] [PubMed]

95. Antunes, A.; Ngugi, D.K.; Stingl, U. Microbiology of the Red Sea (and other) deep-sea anoxic brine lakes. *Environ. Microbiol. Rep.* **2011**, *3*, 416–433. [CrossRef] [PubMed]

96. Blokhuis, A.; Lacoste, D.; Nghe, P.; Peliti, L. Selection Dynamics in Transient Compartmentalization. *Phys. Rev. Lett.* **2018**, *120*, 158101. [CrossRef] [PubMed]

97. Szostak, J.W. The eightfold path to non-enzymatic RNA replication. *J. Syst. Chem.* **2012**, *3*, 2. [CrossRef]

98. He, C.; Gállego, I.; Laughlin, B.; Grover, M.A.; Hud, N.V. A viscous solvent enables information transfer from gene-length nucleic acids in a model prebiotic replication cycle. *Nat. Chem.* **2017**, *9*, 318–324. [CrossRef]

99. Mariani, A.; Bonfio, C.; Johnson, C.M.; Sutherland, J.D. pH-Driven RNA Strand Separation under Prebiotically Plausible Conditions. *Biochemistry* **2018**, *57*, 6382–6386. [CrossRef]

100. Singleton, M.R.; Dillingham, M.S.; Wigley, D.B. Structure and mechanism of helicases and nucleic acid translocases. *Annu. Rev. Biochem.* **2007**, *76*, 23–50. [CrossRef]

101. Krishnamurthy, R. Giving Rise to Life: Transition from Prebiotic Chemistry to Protobiology. *Acc. Chem. Res.* **2017**, *50*, 455–459. [CrossRef]

102. Lubock, N.B.; Zhang, D.; Sidore, A.M.; Church, G.M.; Kosuri, S. A systematic comparison of error correction enzymes by next-generation sequencing. *Nucleic Acids Res.* **2017**, *45*, 9206–9217. [CrossRef]

103. Prévôt, M.E.; Ustunel, S.; Hegmann, E. Liquid Crystal Elastomers-A Path to Biocompatible and Biodegradable 3D-LCE Scaffolds for Tissue Regeneration. *Materials* **2018**, *11*, 377. [CrossRef]

104. Frenkel-Pinter, M.; Samanta, M.; Ashkenasy, G.; Leman, L.J. Prebiotic Peptides: Molecular Hubs in the Origin of Life. *Chem. Rev.* **2020**, *120*, 4707–4765. [CrossRef] [PubMed]

105. Kitadai, N.; Maruyama, S. Origins of building blocks of life: A review. *Geosci. Front.* **2018**, *9*, 1117–1153. [CrossRef]

106. Naskar, S.; Saurabh, S.; Jang, Y.H.; Lansac, Y.; Maiti, P.K. Liquid crystal ordering of nucleic acids. *Soft Matter* **2020**, *16*, 634–641. [CrossRef]

107. Huang, M.; Song, J.; Huang, P.; Chen, X.; Wang, W.; Zhu, Z.; Song, Y.; Yang, C. Molecular Crowding Evolution for Enabling Discovery of Enthalpy-Driven Aptamers for Robust Biomedical Applications. *Anal. Chem.* **2019**, *91*, 10879–10886. [CrossRef] [PubMed]

108. Saad, N.Y. A ribonucleopeptide world at the origin of life: Co-evolution of RNA, amino acids and peptide. *J. Syst. Evol.* **2018**, *56*, 1–13. [CrossRef]

109. Piette, B.M.A.G.; Heddle, J.G. A Peptide-Nucleic Acid Replicator Origin for Life. *Trends Ecol. Evol.* **2020**, *35*, 397–406. [CrossRef]

110. Poudyal, R.R.; Pir Cakmak, F.; Keating, C.D.; Bevilacqua, P.C. Physical Principles and Extant Biology Reveal Roles for RNA-Containing Membraneless Compartments in Origins of Life Chemistry. *Biochemistry* **2018**, *57*, 2509–2519. [CrossRef]

111. Damer, B.; Deamer, D. The Hot Spring Hypothesis for an Origin of Life. *Astrobiology* **2019**, *20*, 429–452. [CrossRef]